Version of Record: https://www.sciencedirect.com/science/article/pii/S0169433221031299
Manuscript_33b458ac7c6ff2e3039078073b7ce38f

Integration of epitaxial $La_{2/3}Sr_{1/3}MnO_3$ thin films on silicon-on-sapphire substrate for MEMS applications

Sandeep Kumar Chaluvadi,[1,2*] Zhe Wang,[3] Laryssa M. Carvalho de Araujo,[1] Pasquale Orgiani,[2,4] Vincent Polewczyk,[2] Giovanni Vinai,[2] Olivier Rousseau,[1] Victor Pierron,[1] Alain Pautrat,[5] B. Domenges,[5] Darrell G. Schlom,[3,6] and Laurence Mechin[1*]

[1]Normandie Univ, UNICAEN, ENSICAEN, CNRS, GREYC, 14000 Caen, France
[2] Istituto Officina dei Materiali (IOM)-CNR, Laboratorio TASC, Area Science Park, S.S. 14 km 163.5, Trieste I-34149, Italy
[3]Department of Materials Science and Engineering, Cornell University, Ithaca, New York 14853-1501, USA
[4]CNR-SPIN, UOS Salerno, 84084 Fisciano, SA, Italy
[5]Normandie Univ, UNICAEN, ENSICAEN, CNRS, CRISMAT, 14050 Caen, France
[6]Kavli Institute at Cornell for Nanoscale Science, Cornell University, Ithaca, New York 14853-1501, USA

*Corresponding author: chaluvadi@iom.cnr.it

*Corresponding author: laurence.mechin@ensicaen.fr

Abstract

We report the integration of high-quality epitaxial $La_{2/3}Sr_{1/3}MnO_3$ (LSMO) thin films onto $SrTiO_3$ buffered Silicon-on-Sapphire (SOS) substrates by combining state-of-the-art thin film growth techniques such as molecular beam epitaxy and pulsed laser deposition. Detailed structural, magnetic and electrical characterizations of the LSMO/STO/SOS heterostructures show that the LSMO film properties are competitive with those directly grown on oxide substrates. X-ray magnetic circular dichroism measurements on Mn $L_{2,3}$ edges show strong dichroic signal at room temperature, and angular-dependent *in-plane* magnetic properties by magneto-optical Kerr magnetometry reveal isotropic magnetic anisotropy. Suspended micro-bridges were thus finally fabricated by silicon micromachining, thus demonstrating the potential use of integrating LSMO magnetic layer on industrially compatible SOS substrates for the development of applicative MEMS devices.

Keywords: **LSMO, manganites, pulsed laser deposition, silicon-on-sapphire, silicon micromachining, suspended bridge, MEMS**

© 2021 published by Elsevier. This manuscript is made available under the Elsevier user license
https://www.elsevier.com/open-access/userlicense/1.0/

1. Introduction

Optimal 'Sr' doped manganite $La_{2/3}Sr_{1/3}MnO_3$ (LSMO) exhibiting a room-temperature ferromagnetic metal phase (Curie temperature, T_c ~ 360 K) [1] is considered as a suitable candidate not only for spintronic devices but also bolometers and microelectromechanical systems (MEMS) [2–5]. LSMO thin films are also used as buffer layers for low field magnetic sensors, magnetic memory applications operating at room temperature [6–8]. Several studies have been made on the LSMO film growth on many oxide substrates showing excellent electrical and magnetic properties of the LSMO films [9–13]. Despite these excellent properties, oxide substrates are considered neither industrially scalable nor economically viable. Therefore, in the last decade, with the advancements in the epitaxial growth techniques such as MBE and PLD, attempts were successfully made to epitaxially grow LSMO films on silicon substrates by using $SrTiO_3$ (STO), $CaTiO_3$ or CeO_2/YSZ as a buffer layer [14–20]. Other techniques such as transfer printing [21] have been also pursued. These advancements in oxide integration on a semiconductor substrate are a great step towards realizing device applications [16]. Along with silicon, there is also an interest in exploring the integration of LSMO on other industrially compatible substrates such as Silicon-on-Insulator (SOI) [22], Silicon-on-Sapphire (SOS), etc. These substrates are known to outperform bulk silicon wafers in the development of RF devices due to their higher insulating properties and are already being used in complementary metal-oxide semiconductor (CMOS) technologies [23]. Sapphire substrates are also advantageous in the development of high-frequency devices, thanks to their low dielectric losses. The combination of silicon with sapphire in SOS substrates additionally allows the use of the conventional micromachining techniques of silicon for the fabrication of MEMS devices. In particular, since the use of SOS substrates offers the double advantage of the use of sapphire as a material with a high dielectric constant for high-frequency operation and of silicon for micromachining these substrates are very promising to be used in the fabrication of antenna-coupled bolometers for infrared or THz detection [24]. Despite the numerous advantages, to our knowledge, no attempts have been made on the integration of manganite films on SOS substrate.

In this paper, we studied the structural, magnetic and electrical properties of epitaxial LSMO films integrated on SOS substrate by using STO as a buffer layer. High quality electrical and magnetic properties were obtained, as confirmed by electrical resistivity and magnetization versus temperature characteristics, but also more advanced techniques such as room temperature

element sensitive x-ray absorption (XAS) and x-ray magnetic circular dichroism (XMCD) spectra at the Mn $L_{2,3}$ edges performed at the advanced photoelectric effect beamline high-energy branch (APE-HE) of the Elettra synchrotron radiation facility in Trieste, Italy [25] and angular-dependent *in-plane* magneto-optical Kerr (MOKE) measurements at NFFA facility in Trieste [26]. Finally, suspended micro-bridges were fabricated by the traditional silicon micromachining technique. The combination of these results shows that LSMO/STO/SOS heterostructures are a valid candidate for the development of room temperature silicon integrated magnetic, bolometric and MEMS devices.

2. Experimental details

STO buffered LSMO thin films were epitaxially grown onto commercially available SOS substrate (from Kyocera) by molecular beam epitaxy (MBE) and pulsed laser deposition (PLD) techniques. The SOS wafers are composed of 700 nm thick silicon on top of 430 μm thick sapphire substrate. At first, a 20 nm STO (001) buffer layer was deposited onto a 3-inch SOS wafer by MBE as previously reported on Si (001) wafers at Cornell, USA [17]. The 3-inch SOS wafer was then diced into several 10×10 mm^2 substrates for the subsequent deposition of films by PLD equipped with *in-situ* reflection high-energy electron diffraction (RHEED) at Caen, France. A KrF excimer laser of wavelength (λ) 248 nm, laser energy density and laser repetition rate of 1.4 – 1.7 J/cm^2 and 1 Hz was used respectively. Prior to 30 or 45 nm thick LSMO deposition, a 2 nm thick STO layer was deposited by PLD on the previously MBE grown 20 nm STO layer in order to obtain a clean STO surface. STO and LSMO films were deposited at 0.1 mbar and 0.17 mbar O_2 partial pressure respectively, with the substrate temperature, maintained at 750°C. After deposition, films were cooled down to room temperature at 10°C per minute rate in 700 mbar O_2 pressure.

XAS spectra were taken at Mn $L_{2,3}$ edges in total electron yield (TEY) mode, at room temperature, in circular polarization. The sample surface was kept with an angle of 45° with respect to the incident beam. The XMCD spectra were measured at remanence, after applying external alternating magnetic field pulses of ±30 mT in the surface plane of the sample at each energy point of the spectra. The applied field was large enough to saturate the sample magnetization. The spectra are therefore normalized to the L_3 edge intensity of the sum of the two spectra. The XMCD signal intensity, coming from the difference of the two spectra, takes into account both the angle of 45° between the photon angular momentum and the sample

magnetization and the 75% degree of polarization of the circular light. Element sensitive hysteresis loops at Mn edge were measured by scanning the magnitude of the applied magnetic field in the range ±8 mT, at both L_3 edge and pre-edge energy values, for both photon helicity. Finally, LSMO suspended micro-bridges were fabricated in class 1000 cleanroom as follows. After the LSMO (45 nm)/STO (2 nm) deposition by PLD on STO(20nm)/SOS, gold contacts were added in a two-stage process by combining PLD and ion beam deposition to avoid degradation of the LSMO film properties. The gold contact pads were defined by means of UV photolithography and etched in KI solution. The photoresist was kept for the PLD deposition at an ambient temperature of a protection layer of about 30 nm thick amorphous STO (a-STO) layer. The double clamped-edge structures were designed in the stack of a-STO/LSMO/STO/SOS by a second UV photolithography step, followed by an ion beam anisotropic etching step down to silicon. Finally, reactive ion etching (RIE) equipped with SF_6 plasma was used to isotropically etch silicon and the bridge structures were released from the substrate.

Figure 1(a) shows the schematic representation of the LSMO/STO/SOS heterostructures along with the thicknesses of the layers and the techniques used for the growth of each layer. Figure 1(b, c) are the RHEED patterns taken along [100] crystallographic direction of STO and LSMO layers. Clear 2D streaks were observed in the RHEED diffraction pattern, indicating the very good crystalline quality of both STO and LSMO layers.

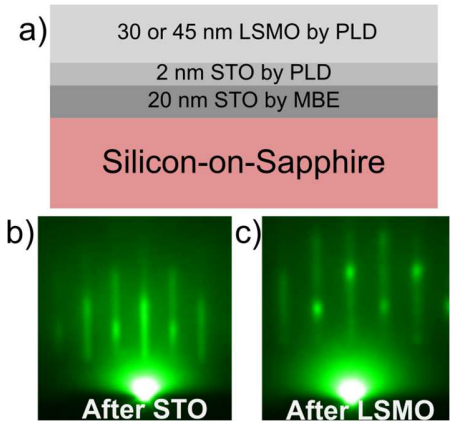

Figure 1: (a) Schematic representation of the 30 or 45 nm thick LSMO on STO/SOS heterostructures, (b and c) RHEED diffraction patterns along [100] direction of STO and LSMO film after deposition at 750 °C, respectively.

3. Results and discussion

3.1. Structural characterization

The crystalline quality and epitaxial relationship between film and substrate were evaluated by a high-resolution four-circle X'Pert X-ray Diffractometer (XRD). Figure 2(a) shows the long-range (20°-90°) θ-2θ XRD scan revealing only (00*l*) orientation, indicating the preferential *c*-axis epitaxial growth of LSMO and STO layers. The diffraction peak present at about 2θ~69° belongs to the silicon (004). The series of (10-12) diffraction peaks from the sapphire substrate indicates that the sapphire crystal is cut along the r-plane. The out-of-plane lattice parameters '*c*' calculated from the θ-2θ XRD for LSMO film and STO buffer layer are 0.383 nm and 0.3905 nm, respectively. As a result, the LSMO film experiences an out-of-plane compressive strain (ε_{zz}) of -1%.

Figure 2(b) shows the omega scan rocking curves taken around the (002) peaks of LSMO and STO, (004) peak of silicon and (20-24) of Sapphire. The full-width half maximum (FWHM) values calculated from the rocking curves of LSMO and STO layers on SOS are ~0.88° and ~0.9° respectively, which is slightly higher than the values reported by our group for LSMO/STO/Si films fully deposited by MBE [17] and similar to other values reported in the literature on Si substrate [14], a sign of high crystalline quality of our thin films. The in-plane epitaxial relationship between film and substrate is determined by asymmetric ϕ-scans around the (013) and (113) peaks of LSMO and Silicon, shown in Figure 2(c). A clear four-fold symmetry with 90° peak separation confirms that the LSMO/STO layers grow in diagonal-on-cube geometry with 45° in-plane rotation on Silicon substrate, owing to the large lattice mismatch between STO (0.3905 nm) and Si (0.534 nm) unit cell parameters. The in-plane and out-of-plane hetero-epitaxial relationship between film and substrate can be viewed as LSMO[100]//STO[100]//Si[110]//Sapphire and LSMO(001)//STO(001)//Si(001)//Sapphire(10-12).

To evaluate the strain in films, asymmetric reciprocal space maps (RSM) (Figure 2(d)) around the (013) reflections of LSMO and STO and (113) of Si were performed. The Qx position of LSMO and STO peaks are aligned vertically, as seen by the solid black line traced in the figure as a guide for the eye, confirming that the LSMO layer is pseudomorphically grown on the

top of STO buffer layer. Whereas, the STO buffer layer tends to relax above a few nanometers thick, as seen from the non-alignment of reciprocal lattice vector position Qx of Si and STO.

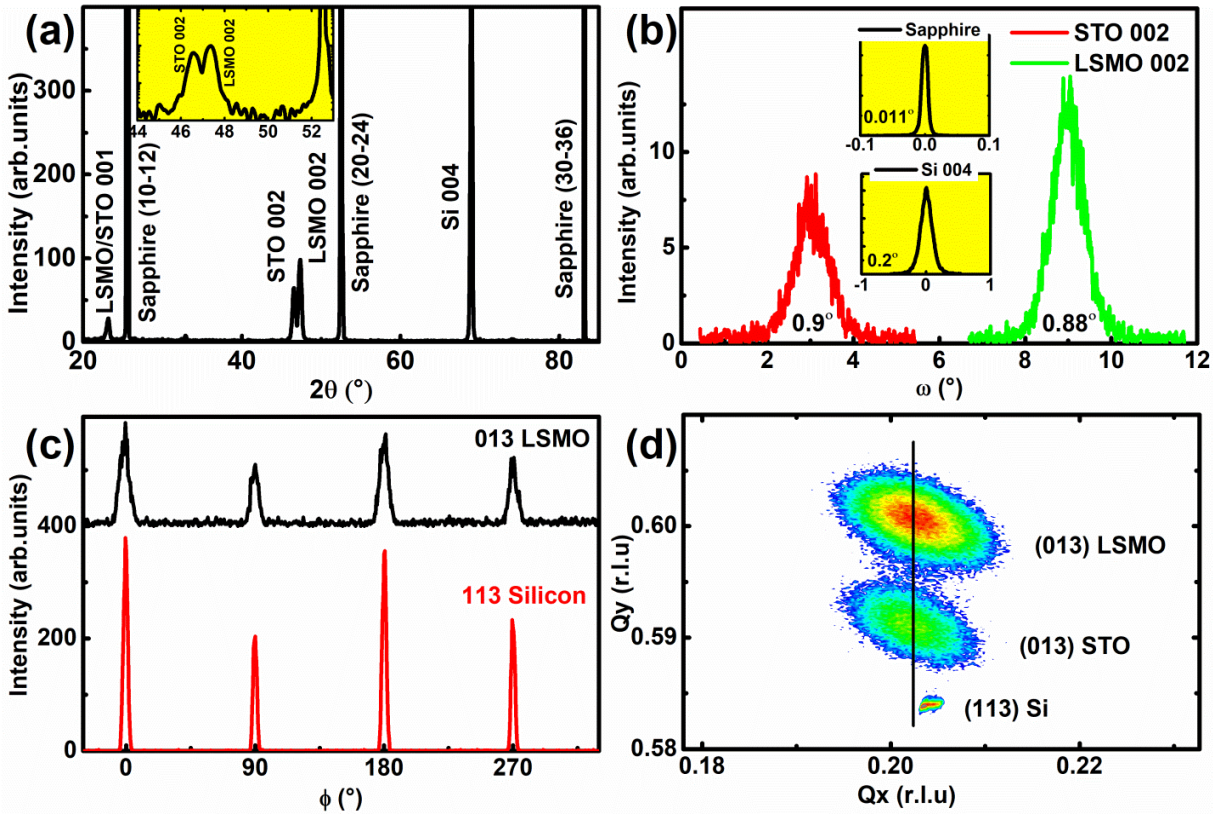

Figure 2: (a) θ-2θ X-ray diffraction pattern (linear scale intensity) of 30 nm LSMO film grown on 20 nm STO buffer layer on the SOS substrate. Inset (log scale intensity) shows the data zoomed around (002) peaks of STO and LSMO layers. (b) Omega scan rocking curves around (20-24) sapphire, (004) silicon, (002) STO and (002) LSMO with FWHM about 0.011°, 0.2°, 0.9° and 0.88° respectively. (c) Asymmetric phi scans around (013) plane of LSMO and (113) of Si, and (d) reciprocal space maps around (013) reflections of LSMO film and STO buffer layer and (113) reflection of Silicon. The solid black line shown as a guide for the eye signifying the peaks of LSMO and STO are aligned vertically.

3.2. Electrical and magnetic properties

To assess the quality of LSMO film integration on industrially compatible SOS substrates, determining the Curie temperature T_C and temperature at maximum resistance (T_P) are key parameters. The temperature dependence of the magnetization M(T) of the film, measured in the temperature range of 10 – 410 K by superconducting quantum interference device (SQUID), with an external magnetic field of 50 mT applied in the film plane, is shown in Figure 3. The film exhibits a typical ferromagnetic behavior and the T_C obtained is ~340 K,

which is similar to the LSMO bulk value [27]. Other studies have reported lower T_C~218 K for LSMO grown on SiO_x/Si, owing to random in-plane misorientations and the presence of nano-region sized disordered phase boundaries [28]. The temperature-dependent (77 – 420 K) electrical resistivity of LSMO film performed by the standard four-probe method is shown in the inset of Figure 3. Interestingly, the film exhibits very low residual resistivity i.e., $\rho < 20$ μΩ-m at 77 K and $\rho < 50$ μΩ-m at 300 K and the temperature coefficient of resistance (TCR) is ~1.6±0.2 K^{-1}. The temperature at maximum resistance (T_p) also displays well above 420 K. Such low resistivity values and very high T_P are comparable to the films grown on various oxide substrates as STO, $NdGaO_3$ (NGO), $(LaAlO_3)_{0.3}(Sr_2TaAlO_6)_{0.7}$ (LSAT) [12,29], thus, confirming the very good integration quality of STO buffered LSMO films on SOS substrate.

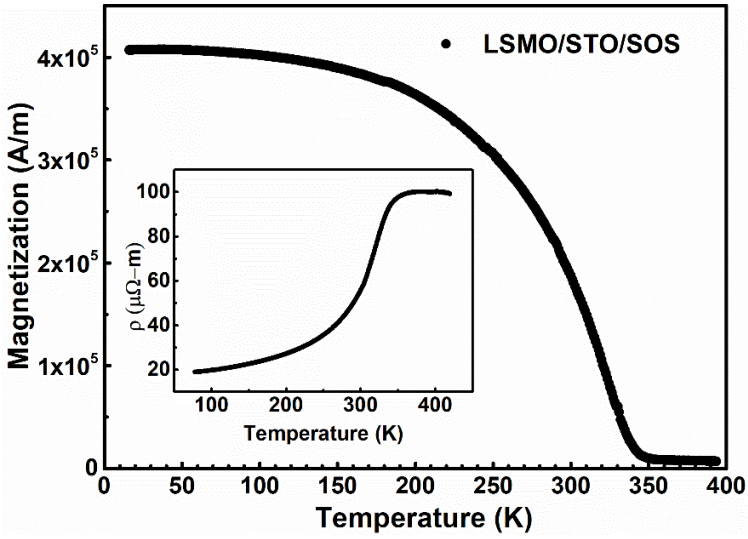

Figure 3: Temperature-dependent magnetization M(T) curve of 30 nm LSMO film on STO buffered SOS substrate, with Tc~340 K. Inset shows temperature-dependent electrical resistivity for the same.

To disclose the nature of magnetic anisotropy present in the LSMO/STO/SOS system, we have studied angular dependent *in-plane* magnetic properties using longitudinal MOKE at 300 K. The sample is rotated in its surface plane while keeping fixed the applied external magnetic field. Figure 4 shows the normalized Kerr hysteresis loops measured along [100], [110] and [010] crystallographic axis of LSMO, which display similar hysteretic behavior without any substantial differences in both remanence magnetization and coercive fields. The polar plot in the inset of Figure 4 shows how the coercivity remains almost constant along with all in-plane directions, with a value of around 3 mT, a sign of an isotropic *in-plane* magnetic property [30].

Such a magnetically isotropic system is ideal for technological applications; as the magnetization direction can be tuned for example, by inducing shape effects through the lithography process [31–33].

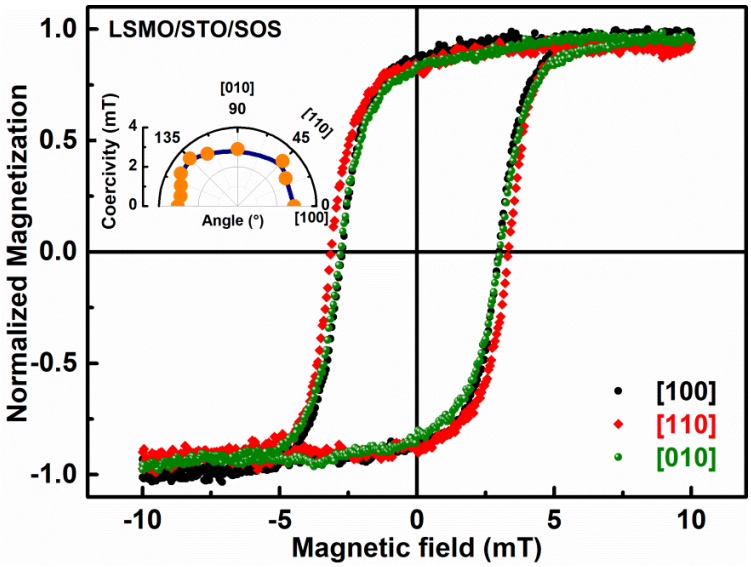

Figure 4: Room temperature angular-dependent in-plane MOKE hysteresis loops of LSMO film deposited on STO buffered SOS substrate. Inset shows its angular-dependent coercivity.

Figure 5(a) shows the XAS and XMCD spectra of 30 nm LSMO film taken at Mn $L_{2,3}$ edges at room temperature. The sample surface was kept with an angle of 45° with respect to the incident beam as shown in the schematic (Inset of Figure 5(a)). XAS technique is very sensitive to subtle changes in electronic structure. Therefore, the presence of Mn^{2+} in the film surface is easily identified by the large intensity absorption peak at ~641 eV [34]. Since such a sharp intense peak is absent around ~641 eV in the XAS spectra (Figure 5), confirming that the surface properties are representative with respect to the bulk of the film [35,36].

The surface of the LSMO shows a clear ferromagnetic signal (Figure 5(a)) with the observed XMCD curve similar to those reported in the literature for epitaxial LSMO films [37,38]. The dichroic signal of 5.4% is observed; indicating that the STO buffered LSMO films on SOS substrate is ferromagnetic at room temperature. The element sensitive hysteresis loop, as shown in Figure 5(b), confirms the ferromagnetic behavior of LSMO at room temperature with a coercive field of 2.3 mT, slightly lower than the coercive field obtained from the MOKE.

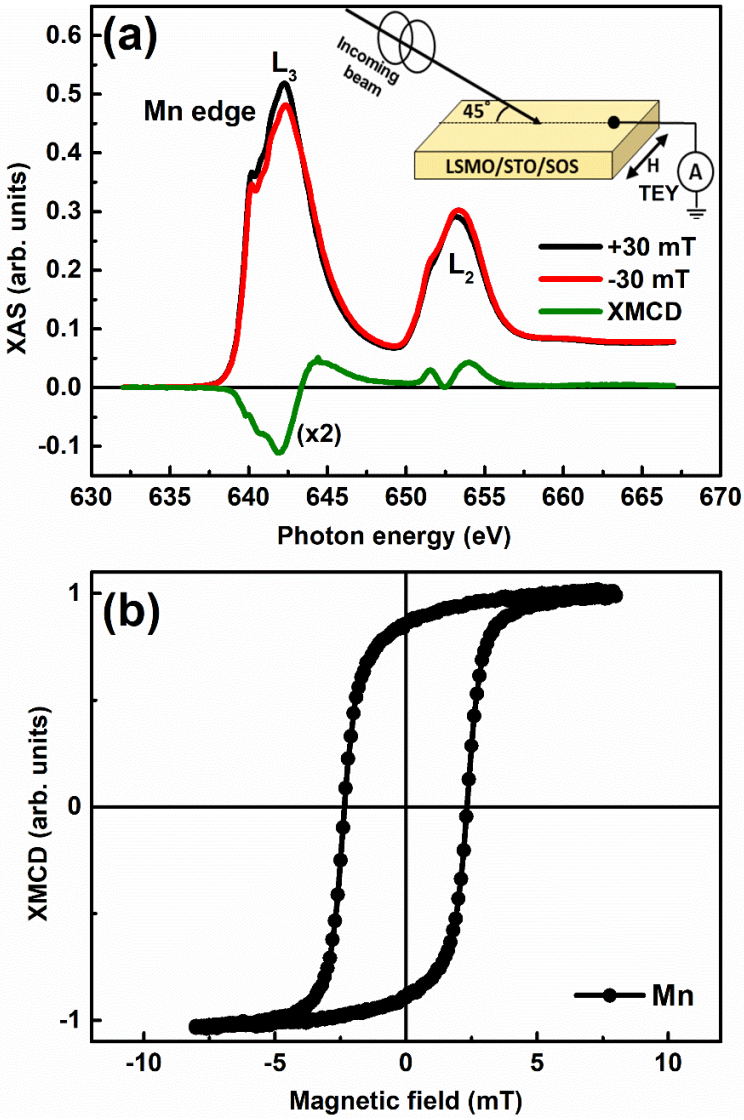

Figure 5: (a) Room-temperature XAS and XMCD results of 30 nm LSMO/STO/SOS substrate with an in-plane applied magnetic field. The experimental configuration is shown in the inset. The XMCD results are reported as a difference of the XAS measurements. (b) Normalized Hysteresis loops of LSMO film taken at the Mn L_3 edge.

3.3. Double clamped-edge structures.

In order to check the possible use of the LSMO/STO/SOS heterostructures for future devices, a successful attempt has been made in fabricating double clamped-edge structures by using the same fabrication process as described in [39]. Figure 6(a) shows a 3D-reconstruction image by digital holographic microscopy (DHM-R2200) of a 3 µm wide × 100 µm long suspended bridge. Suspended bridges of widths up to 6 µm has been fabricated sofar, in line with

our previous experience in the LSMO suspended bridge fabrication on silicon substrates [40]. The thickness profile presented in figure 6(d) at the position shown in the 2D DHM image of figure 6(b) confirms that the full a-STO/LSMO/STO/Si stack was etched since the measured step was 800 nm. The optical microscope image in figure 6(c) shows the same 3 µm wide × 100 µm long suspended bridge with the white color corresponding to lateral etching underneath the a-STO/LSMO/STO/Si. Here the silicon etching rate was about 0.4 $\mu m \cdot min^{-1}$ in depth and 0.1 $\mu m \cdot min^{-1}$ in the horizontal direction. Several 3 µm wide LSMO suspended bridges with different bridge length dimensions (50 µm – 200 µm) were fabricated on the same wafer. The electrical resistance at room temperature measured using 4 probes was 10.5 kΩ, 17.6 kΩ, 27.6 kΩ and 35.6 kΩ, for the 50, 100, 150 and 200 µm long suspended bridges respectively, thus leading to electrical resistivity in the range of 24 - 28 µΩ·m. Such low resistivity values obtained for the suspended micro-bridge structures further stress that the quality of the LSMO magnetic layer is not degraded even after several lithographic process steps. In further studies, it can be essential to investigate how the electrical resistivity depends on the geometry of the suspended structures.

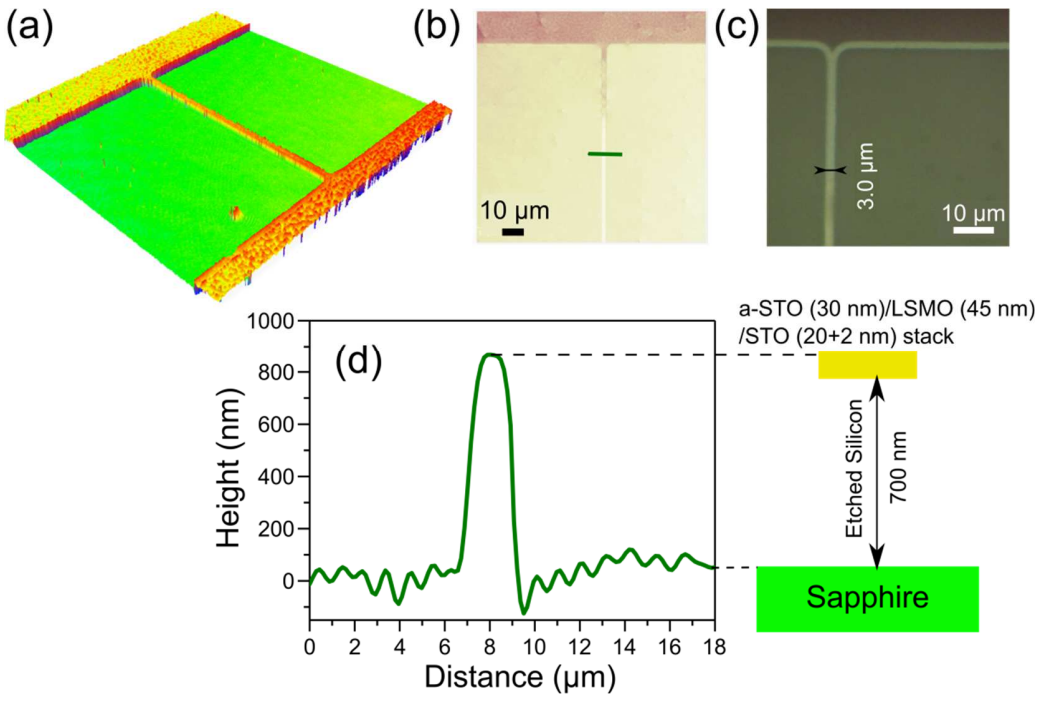

Figure 6: (a) 3D-reconstruction DHM image, (b) 2D DHM image and (c) optical microscope image of a 3 µm wide 100 µm long suspended bridge; (d) Thickness profile at the position shown in the 2D DHM image of (b) with the schematic cross-section of the suspended a-STO/LSMO/STO stack.

4. Conclusion

We integrated epitaxial LSMO magnetic oxide perovskite layer on industrial compatible SOS wafers by combining MBE and PLD techniques and by using STO as a buffer layer. The structural, electrical (T_P > 420 K) and magnetic properties (T_C ~ 340 K) of the LSMO on SOS were found to be comparable with those of LSMO films deposited on various oxide substrates. Angular-dependent *in-plane* magnetic measurements by MOKE show an isotropic behavior. Finally, a successful attempt has been made in fabricating LSMO oxide-based suspended micro-bridge structures on SOS wafers by the traditional silicon micromachining technique. The low resistivity of micro-bridges 24 - 28 μΩ·m confirms that our lithography process methodology still preserves the epitaxial quality of the LSMO layer. Hence, the LSMO/STO/SOS based system may thus represent the new strategy in integrating multifunctional oxides on industrial compatible wafers, opening the way for innovative electrical/magnetic and MEMS device applications.

Acknowledgements

This work was supported by the Normandy region through a doctoral grant for L.M.C.A. L.M. is grateful to J.C. Villégier who provided the SOS substrates. This work has been partially performed in the framework of the Nanoscience Foundry and Fine Analysis (NFFA-MUR Italy Progetti Internazionali) project (www.trieste.NFFA.eu).

Conflict of Interest

The authors declare that they have no known competing financial interests or personal relationships that could have appeared to influence the work reported in this paper.

Author contributions

CRediT authorship contribution statement

Sandeep Kumar Chaluvadi: Conceptualization, Investigation, Data curation, Writing-Original draft preparation, **Zhe wang:** Investigation, Validation, **Laryssa M. Carvalho:** Conceptualization, Formal analysis, Investigation, **Pasquale Orgiani:** Conceptualization, Validation, Supervision, Writing-Reviewing and Editing, **Vincent Polewczyk:** Investigation, Visualization, **Giovanni Vinai:** Validation, **Olivier Rousseau:** Verification, Writing-Reviewing

and Editing, **Victor Pierron:** Resources, **Alain Pautrat:** Validation, **B.Domenges:** Investigation, **Darrell G. Schlom:** Supervision, **Laurence Mechin:** Supervision

References

[1] Y. Tokura, Y. Tomioka, Colossal magnetoresistive manganites, J. Magn. Magn. Mater. 200 (1999) 1–23. https://doi.org/10.1016/S0304-8853(99)00352-2.

[2] M. Bibes, A. Barthélémy, Oxide spintronics, IEEE Trans. Electron Devices. 54 (2007) 1003–1023. https://doi.org/10.1109/TED.2007.894366.

[3] L.G. Enger, S. Flament, I.-N. Bhatti, B. Guillet, M.L.C. Sing, V. Pierron, S. Lebargy, J.M. Diez, A. Vera, I. Martinez, R. Guerrero, L. Perez, P. Perna, J. Camarero, R. Miranda, M.T. Gonzalez, L. Mechin, Sub-nT resolution of Single Layer Sensor Based on the AMR Effect in La2/3Sr1/3MnO3 Thin Films, IEEE Trans. Magn. X (2021) 1–1. https://doi.org/10.1109/TMAG.2021.3089373.

[4] V.M. Nascimento, L. Méchin, S. Liu, A. Aryan, C. Adamo, D.G. Schlom, B. Guillet, Electro-thermal and optical characterization of an uncooled suspended bolometer based on an epitaxial La0.7Sr0.3MnO3 film grown on CaTiO3/Si, J. Phys. D. Appl. Phys. 54 (2020) 055301. https://doi.org/10.1088/1361-6463/ABBFCA.

[5] D. Le Bourdais, G. Agnus, T. Maroutian, V. Pillard, P. Aubert, R. Bachelet, G. Saint-Girons, B. Vilquin, E. Lefeuvre, P. Lecoeur, Epitaxial manganite freestanding bridges for low power pressure sensors, J. Appl. Phys. 118 (2015) 124509. https://doi.org/10.1063/1.4931885.

[6] Y. Bason, L. Klein, J.-B. Yau, X. Hong, J. Hoffman, C.H. Ahn, Planar Hall-effect magnetic random access memory, J. Appl. Phys. 99 (2006) 08R701. https://doi.org/10.1063/1.2162824.

[7] J. Hoffman, X. Hong, C.H. Ahn, Device performance of ferroelectric/correlated oxide heterostructures for non-volatilememory applications, Nanotechnology. 22 (2011) 254014. https://doi.org/10.1088/0957-4484/22/25/254014.

[8] M. Bibes, J.E. Villegas, A. Barthélèmy, Ultrathin oxide films and interfaces for electronics and spintronics, Adv. Phys. 60 (2011) 5–84. https://doi.org/10.1080/00018732.2010.534865.

[9] A.Y. Petrov, C. Aruta, S. Mercone, C. Adamo, I. Alessandri, L. Maritato, Room temperature metal-insulator transition in as grown (La 1-xSrx)yMnO3 thin films deposited

by molecular beam epitaxy, Eur. Phys. J. B. 40 (2004) 11–17. https://doi.org/10.1140/epjb/e2004-00233-7.

[10] C. Adamo, X. Ke, H.Q. Wang, H.L. Xin, T. Heeg, M.E. Hawley, W. Zander, J. Schubert, P. Schiffer, D. a. Muller, L. Maritato, D.G. Schlom, Effect of biaxial strain on the electrical and magnetic properties of (001) La0.7Sr0.3MnO3 thin films, Appl. Phys. Lett. 95 (2009) 112504. https://doi.org/10.1063/1.3213346.

[11] F. Tsui, M.C. Smoak, T.K. Nath, C.B. Eom, Strain-dependent magnetic phase diagram of epitaxial La0.67Sr0.33MnO3 thin films, Appl. Phys. Lett. 76 (2000) 2421–2423. https://doi.org/10.1063/1.126363.

[12] S.K. Chaluvadi, F. Ajejas, P. Orgiani, S. Lebargy, A. Minj, S. Flament, J. Camarero, P. Perna, L. Méchin, Epitaxial strain and thickness dependent structural, electrical and magnetic properties of La 0.67 Sr 0.33 MnO 3 films, J. Phys. D. Appl. Phys. 53 (2020) 375005. https://doi.org/10.1088/1361-6463/ab8e7b.

[13] S.K. Chaluvadi, P. Perna, F. Ajejas, J. Camarero, A. Pautrat, S. Flament, L. Méchin, Thickness and angular dependent magnetic anisotropy of La 0.67 Sr 0.33 MnO 3 thin films by Vectorial Magneto Optical Kerr Magnetometry, J. Phys. Conf. Ser. 903 (2017) 012021. https://doi.org/10.1088/1742-6596/903/1/012021.

[14] J. Manuel Vila-Fungueiriño, J. Gázquez, C. Magen, G. Saint-Girons, R. Bachelet, A. Carretero-Genevrier, Epitaxial La0.7Sr0.3MnO3 thin films on silicon with excellent magnetic and electric properties by combining physical and chemical methods, Sci. Technol. Adv. Mater. Natl. Inst. Mater. Sci. 19 (2018) 702–710. https://doi.org/10.1080/14686996.2018.1520590ï.

[15] S.H. Baek, C.B. Eom, Epitaxial integration of perovskite-based multifunctional oxides on silicon, Acta Mater. 61 (2013) 2734–2750. https://doi.org/10.1016/j.actamat.2012.09.073.

[16] D.P. Kumah, J.H. Ngai, L. Kornblum, Epitaxial Oxides on Semiconductors: From Fundamentals to New Devices, Adv. Funct. Mater. 30 (2020) 1901597. https://doi.org/10.1002/adfm.201901597.

[17] L. Méchin, C. Adamo, S. Wu, B. Guillet, S. Lebargy, C. Fur, J.-M. Routoure, S. Mercone, M. Belmeguenai, D.G. Schlom, Epitaxial La0.7Sr0.3MnO3 thin films grown on SrTiO3 buffered silicon substrates by reactive molecular-beam epitaxy, Phys. Status Solidi. 209 (2012) 1090–1095. https://doi.org/10.1002/PSSA.201127712.

[18] T. Parkelj Potočnik, E. Zupanič, W.Y. Tong, E. Bousquet, D. Diaz Fernandez, G. Koster,

P. Ghosez, M. Spreitzer, Atomic structure of Sr/Si(0 0 1)(1 × 2) surfaces prepared by Pulsed laser deposition, Appl. Surf. Sci. 471 (2019) 664–669. https://doi.org/10.1016/J.APSUSC.2018.12.027.

[19] C. Adamo, L. Méchin, T. Heeg, M. Katz, S. Mercone, B. Guillet, S. Wu, J.-M. Routoure, J. Schubert, W. Zander, R. Misra, P. Schiffer, X.Q. Pan, D.G. Schlom, Enhanced electrical and magnetic properties in La0.7Sr0.3MnO3 thin films deposited on CaTiO3-buffered silicon substrates, APL Mater. 3 (2015) 062504. https://doi.org/10.1063/1.4915486.

[20] P. Perna, L. Méchin, M.P. Chauvat, P. Ruterana, C. Simon, U. Scotti di Uccio, High Curie temperature for La(0.7)Sr(0.3)MnO(3) thin films deposited on CeO(2) /YSZ-based buffered silicon substrates., J. Phys. Condens. Matter. 21 (2009) 306005. https://doi.org/10.1088/0953-8984/21/30/306005.

[21] C.-C. Chiu, Y.-W. Chang, Y.-C. Shao, Y.-C. Liu, J.-M. Lee, S.-W. Huang, W. Yang, J. Guo, F.M. de Groot, J.-C. Yang, Y.-D. Chuang, Spectroscopic characterization of electronic structures of ultra-thin single crystal La0.7Sr0.3MnO3, Sci. Rep. 11 (2021) 5250. https://doi.org/10.1038/S41598-021-84598-8.

[22] Š. Chromik, V. Štrbík, E. Dobročka, T. Roch, A. Rosová, M. Španková, T. Lalinský, G. Vanko, P. Lobotka, M. Ralbovský, P. Choleva, LSMO thin films with high metal–insulator transition temperature on buffered SOI substrates for uncooled microbolometers, Appl. Surf. Sci. 312 (2014) 30–33. https://doi.org/10.1016/J.APSUSC.2014.05.051.

[23] D. Kelly, C. Brindle, C. Kemerling, M. Stuber, The state-of-the-art of silicon-on-sapphire CMOS RF switches, Tech. Dig. - IEEE Compd. Semicond. Integr. Circuit Symp. CSIC. (2005) 200–203. https://doi.org/10.1109/CSICS.2005.1531812.

[24] H.H. Yang, G.M. Rebeiz, Sub-10 pW/Hz0.5 room temperature Ni nano-bolometer, Appl. Phys. Lett. 108 (2016) 053106. https://doi.org/10.1063/1.4940975.

[25] G. Panaccione, I. Vobornik, J. Fujii, D. Krizmancic, E. Annese, L. Giovanelli, F. MacCherozzi, F. Salvador, A. De Luisa, D. Benedetti, A. Gruden, P. Bertoch, F. Polack, D. Cocco, G. Sostero, B. Diviacco, M. Hochstrasser, U. Maier, D. Pescia, C.H. Back, T. Greber, J. Osterwalder, M. Galaktionov, M. Sancrotti, G. Rossi, Advanced photoelectric effect experiment beamline at Elettra: A surface science laboratory coupled with Synchrotron Radiation, Rev. Sci. Instrum. 80 (2009) 043105. https://doi.org/10.1063/1.3119364.

[26] G. Vinai, F. Motti, A.Y. Petrov, V. Polewczyk, V. Bonanni, R. Edla, B. Gobaut, J. Fujii,

F. Suran, D. Benedetti, F. Salvador, A. Fondacaro, G. Rossi, G. Panaccione, B.A. Davidson, P. Torelli, An integrated ultra-high vacuum apparatus for growth and in situ characterization of complex materials, Rev. Sci. Instrum. 91 (2020) 085109. https://doi.org/10.1063/5.0005302.

[27] A. Urushibara, Y. Moritomo, T. Arima, A. Asamitsu, G. Kido, Y. Tokura, Insulator-metal transition and giant magnetoresistance in La1-xSrxMnO3, Phys. Rev. B. 51 (1995) 14103–14109. https://doi.org/10.1103/PhysRevB.51.14103.

[28] M.C. Ramírez Camacho, C.F. Sánchez Valdés, M. Curiel, J.L. Sánchez Llamazares, J.M. Siqueiros, O. Raymond Herrera, Superparamagnetic state in La0.7Sr0.3MnO3 thin films obtained by rf-sputtering, Sci. Rep. 10 (2020) 1–11. https://doi.org/10.1038/s41598-020-59334-3.

[29] S.K. Chaluvadi, F. Ajejas, P. Orgiani, O. Rousseau, G. Vinai, A.Y. Petrov, P. Torelli, A. Pautrat, J. Camarero, P. Perna, L. Mechin, Room temperature biaxial magnetic anisotropy in La 0.67 Sr 0.33 MnO 3 thin films on SrTiO 3 buffered MgO (001) substrates for spintronic applications, Appl. Phys. Lett. 113 (2018) 052403. https://doi.org/10.1063/1.5020072.

[30] S.K. Chaluvadi, Influence of the epitaxial strain on magnetic anisotropy in LSMO thin films for spintronics applications, Normandie Université English (NNT : 2017NORMC248), 2017. https://doi.org/https://tel.archives-ouvertes.fr/tel-01717569.

[31] J. Pawlak, A. Żywczak, J. Kanak, M. Przybylski, Surface-Step-Induced Magnetic Anisotropy in Epitaxial LSMO Deposited on Engineered STO Surfaces, Mater. 2020, Vol. 13, Page 4148. 13 (2020) 4148. https://doi.org/10.3390/MA13184148.

[32] H. Mishra, M. Hehn, D. Lacour, O. Elmazria, N. Tiercelin, H. Mjahed, K. Dumesnil, S.P. Watelot, V. Polewczyk, A. Talbi, O.B. Matar, S. Hage-Ali, Intrinsic versus shape anisotropy in micro-structured magnetostrictive thin films for magnetic surface acoustic wave sensors, Smart Mater. Struct. 28 (2019) 12LT01. https://doi.org/10.1088/1361-665X/AB522D.

[33] V. Polewczyk, G. Vinai, F. Motti, S. Dal Zilio, P. Capaldo, M. Sygletou, S. Benedetti, G. Rossi, P. Torelli, Original design of a patterned multiferroic heterostructure for electrical control of the magnetic shape anisotropy, J. Magn. Magn. Mater. 507 (2020) 166816. https://doi.org/10.1016/J.JMMM.2020.166816.

[34] S. Valencia, A. Gaupp, W. Gudat, L. Abad, L. Balcells, B. Martínez, Impact of

microstructure on the Mn valence of La2/3 Ca1/3Mn O3 thin films, Phys. Rev. B - Condens. Matter Mater. Phys. 75 (2007) 184431. https://doi.org/10.1103/PhysRevB.75.184431.

[35] P. Orgiani, A. Galdi, C. Aruta, V. Cataudella, G. De Filippis, C.A. Perroni, V. Marigliano Ramaglia, R. Ciancio, N.B. Brookes, M. Moretti Sala, G. Ghiringhelli, L. Maritato, Multiple double-exchange mechanism by Mn2⊃+ doping in manganite compounds, Phys. Rev. B - Condens. Matter Mater. Phys. 82 (2010) 1–6. https://doi.org/10.1103/PhysRevB.82.205122.

[36] M.P. De Jong, I. Bergenti, V.A. Dediu, M. Fahlman, M. Marsi, C. Taliani, Evidence for Mn 2+ ions at surfaces of La 0. 7 Sr 0.3 MnO 3 thin films, Phys. Rev. B - Condens. Matter Mater. Phys. 71 (2005) 2–5. https://doi.org/10.1103/PhysRevB.71.014434.

[37] J.H. Park, E. Vescovo, H.J. Kim, C. Kwon, R. Ramesh, T. Venkatesan, Magnetic properties at surface boundary of a half-metallic ferromagnet La 0.7 Sr 0.3 MnO 3, Phys. Rev. Lett. 81 (1998) 1953–1956. https://doi.org/10.1103/PhysRevLett.81.1953.

[38] F. Motti, G. Vinai, A. Petrov, B.A. Davidson, B. Gobaut, A. Filippetti, G. Rossi, G. Panaccione, P. Torelli, Strain-induced magnetization control in an oxide multiferroic heterostructure, Phys. Rev. B. 97 (2018) 1–9. https://doi.org/10.1103/PhysRevB.97.094423.

[39] S. Liu, B. Guillet, C. Adamo, V.M. Nascimento, S. Lebargy, G. Brasse, F. Lemarié, J. El Fallah, D.G. Schlom, L. Méchin, Free-standing La 0.7 Sr 0.3 MnO 3 suspended micro-bridges on buffered silicon substrates showing undegraded low frequency noise properties, J. Micromechanics Microengineering. 29 (2019) 065008. https://doi.org/10.1088/1361-6439/ab16ac.

[40] S. Liu, B. Guillet, C. Adamo, V.M. Nascimento, S. Lebargy, G. Brasse, F. Lemarié, J. El Fallah, D.G. Schlom, L. Méchin, Free-standing La0.7Sr0.3MnO3 suspended micro-bridges on buffered silicon substrates showing undegraded low frequency noise properties, J. Micromechanics Microengineering. 29 (2019) 065008. https://doi.org/10.1088/1361-6439/AB16AC.

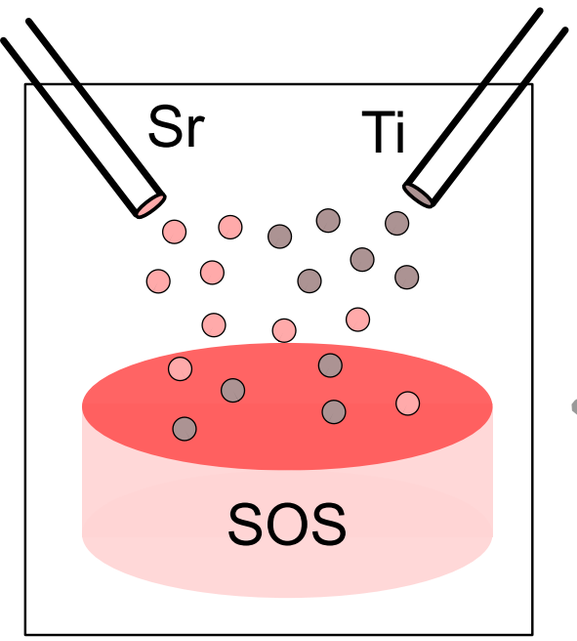

STO buffer layer
by MBE

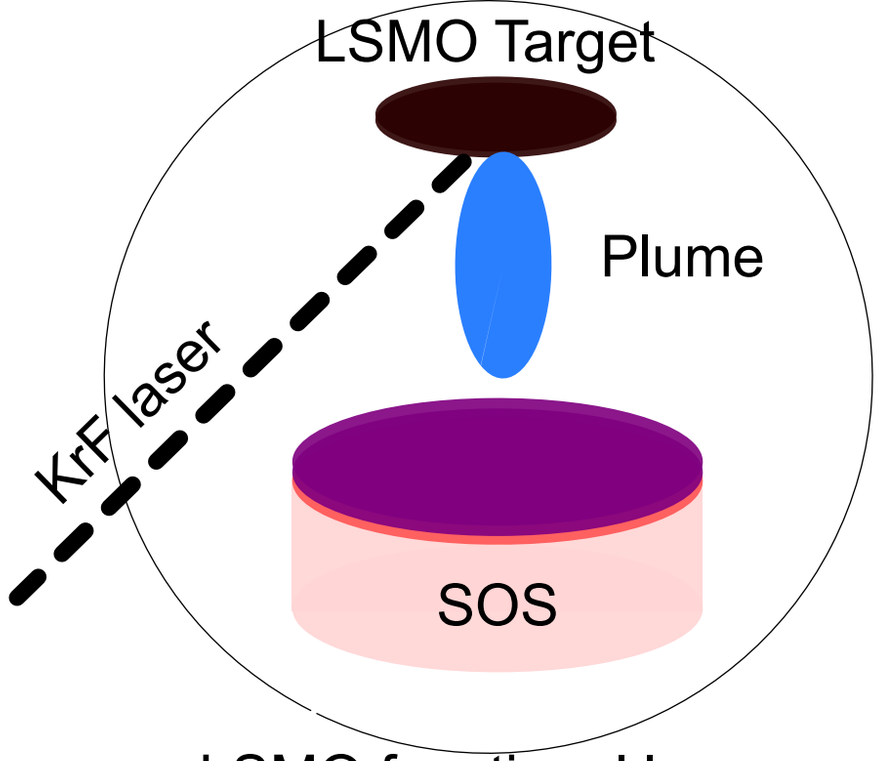

LSMO functional layer
by PLD

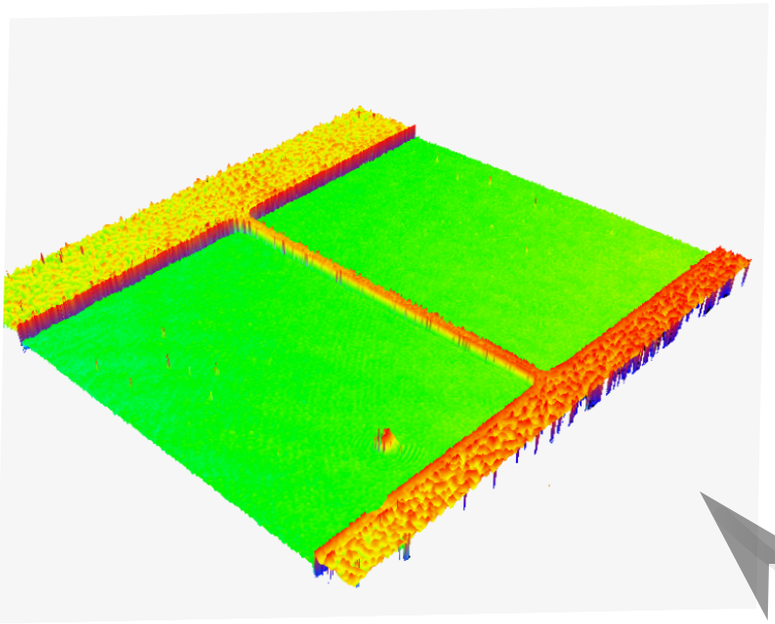

LSMO Suspended
Microbridge

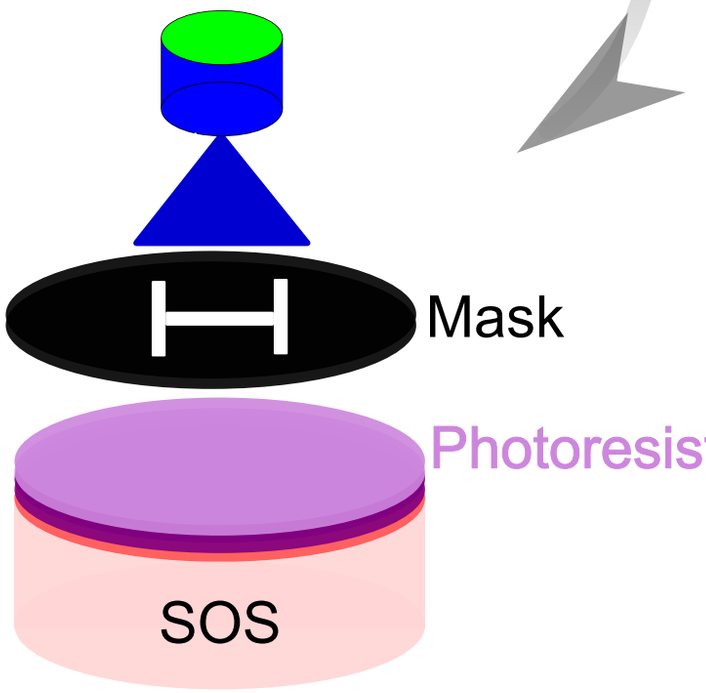

UV Photolithography